LEVEL II

12

AD A108680

AFGL-TR-81-0231
ENVIRONMENTAL RESEARCH PAPERS, NO. 751

A "Worst Case" Spacecraft Environment as Observed by SCATHA on 24 April 1979

E. G. MULLEN
M. S. GUSSENHOVEN
H. B. GARRETT

31 July 1981

SPACE PHYSICS DIVISION PROJECT 7661
AIR FORCE GEOPHYSICS LABORATORY
HANSCOM AFB, MASSACHUSETTS 01731

AIR FORCE SYSTEMS COMMAND, USAF

This report has been reviewed by the ESD Information Office (OI) and is releasable to the National Technical Information Service (NTIS).

This technical report has been reviewed and
is approved for publication.

FOR THE COMMANDER

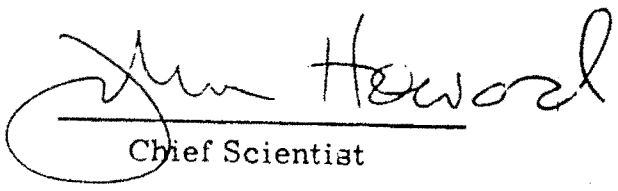

Chief Scientist

Qualified requestors may obtain additional copies from the Defense Documentation Center. All others should apply to the National Technical Information Service.

Unclassified

SECURITY CLASSIFICATION OF THIS PAGE (When Data Entered)

REPORT DOCUMENTATION PAGE	READ INSTRUCTIONS BEFORE COMPLETING FORM
1. REPORT NUMBER: AFGL-TR-81-0231	2. GOVT ACCESSION NO.: AD-A109680
3. RECIPIENT'S CATALOG NUMBER:	
4. TITLE (and Subtitle): A "WORST CASE" SPACECRAFT ENVIRONMENT AS OBSERVED BY SCATHA ON 24 APRIL 1979	5. TYPE OF REPORT & PERIOD COVERED: Scientific. Interim.
	6. PERFORMING ORG. REPORT NUMBER: ERP No. 751
7. AUTHOR(s): E. G. Mullen, M. S. Gussenhoven*, H. B. Garrett**	8. CONTRACT OR GRANT NUMBER(s):
9. PERFORMING ORGANIZATION NAME AND ADDRESS: Air Force Geophysics Laboratory (PHK), Hanscom AFB, Massachusetts 01731	10. PROGRAM ELEMENT, PROJECT, TASK AREA & WORK UNIT NUMBERS: 62101F, 76610803
11. CONTROLLING OFFICE NAME AND ADDRESS: Air Force Geophysics Laboratory (PHK), Hanscom AFB, Massachusetts 01731	12. REPORT DATE: 31 July 1981
	13. NUMBER OF PAGES: 38
14. MONITORING AGENCY NAME & ADDRESS (if different from Controlling Office)	15. SECURITY CLASS. (of this report): Unclassified
	15a. DECLASSIFICATION DOWNGRADING SCHEDULE

16. DISTRIBUTION STATEMENT (of this Report)

Approved for public release; distribution unlimited.

17. DISTRIBUTION STATEMENT (of the abstract entered in Block 20, if different from Report)

18. SUPPLEMENTARY NOTES

*Boston College, Chestnut Hill, Massachusetts

**Jet Propulsion Laboratory, Pasadena, California

19. KEY WORDS (Continue on reverse side if necessary and identify by block number)

Spacecraft charging
SCATHA
Spacecraft environment
Plasma currents

20. ABSTRACT (Continue on reverse side if necessary and identify by block number)

A survey of data from the first year of the P78-2 SCATHA satellite operations showed that a highest level spacecraft frame charging (ϕ_f) both in sunlight (-340 V) and in eclipse (> -8 kV) occurred on 24 April 1979. Analysis of the data indicates that if the sunlight charging environment had been present during eclipse, the vehicle would have charged in excess of 15 kV which is above any known charging level observed to date for the SCATHA satellite. Therefore, the environment at the peak of the sunlight charging at ~0650 UT 24 April 1979 was chosen for this "worst case" study. The environment at this

DD FORM 1 JAN 73 1473

Unclassified

SECURITY CLASSIFICATION OF THIS PAGE (When Data Entered)

20. (Cont)

time is characterized by an injection of high energy (30-335 keV) electron fluxes whose combined current correlates with ϕ_f with a correlation coefficient of 0.95. The fluxes were highly anisotropic, maximizing perpendicular to the magnetic field. The low energy (< 4 keV) electron population had a density < 1 cm^{-3} and the low energy ions were near background. The measured electron distribution functions, when fit to double Maxwellians by a least squares technique, show that throughout the sunlight charging the high and low temperatures remained nearly the same, while the density of the high energy component followed the charging levels. The injection occurred simultaneously with the rapid return of the magnetospheric magnetic field to a more dipole-like configuration.

Preface

Many people have contributed to this effort without whose inputs this report could not have been written. For those staff members at the various contract organizations who work in the shadows and whose names do not appear, a heartfelt thanks. The authors would also like to thank the SCATHA experimenters: D.A. Hardy, AFGL; T.L. Aggson, NASA Goddard; B.G. Ledley, NASA Goddard; E.C. Whipple, UCSD: P.F. Mizera, Aerospace; J.F. Fenell, Aerospace; R.G. Johnson, Lockheed; J.B. Reagan, Lockheed; H.C. Koons, Aerospace; and R.C. Adamo, SRI for use of their data and the countless discussions of its interpretation. A special thanks to D.E. Delorey of Boston College who endured numerous computer program modifications to give us a quality product, and to his contract monitor, Mr. R.E. McInerney of AFGL who provided us the necessary computer resources to accomplish the task. Thanks also to N. Heinemann of Boston College for data presentations, L. Cassidy of Regis College for graphics and artwork, and J. Cronin of AFGL for his computer graphics and statistical analysis. The work of M.S. Gussenhoven was supported by the Air Force Geophysics Laboratory under Contract F19628-79-C-0031.

Contents

Illustrations

Tables

Tables

A "Worst Case" Spacecraft Environment as Observed by SCATHA on 24 April 1979

1. INTRODUCTION

Because spacecraft at geosynchronous orbits can charge to levels significant enough to impact and degrade system performance, there is a need for space vehicle design engineers to have a "worst case" charging environment. However, a definition of "worst case" has been somewhat elusive. Proposed definitions include: (a) the measured environment which produces the largest vehicle frame (ground) to plasma potential difference (ϕ_f), (b) the environment which produces the largest differential potential between adjacent spacecraft surface materials, (c) the hottest plasma environment encountered at geosynchronous orbit, and (d) the environment which causes the greatest number of satellite anomalies. For this study, a "worst case" environment which fulfills some of the above criteria will be discussed. The case presented here is from data taken on the Spacecraft Charging AT High Altitudes (SCATHA) satellite on 24 April 1979. The SCATHA data are from the most complete instrumentation complement flown to date for studying spacecraft charging effects.

The "worst case" described here is a sunlight charging event, although the data extend into satellite eclipse. In eclipse, the satellite potential severely affects the ion and electron spectra inhibiting an accurate measurement of the ambient particles. In sunlight, the satellite potential is much smaller since photoelectrons

(Received for publication 29 July 1981)

provide a significant amount of the current balance and the particle spectra are affected to a much lesser degree. Estimates of the satellite potential, had the vehicle been in eclipse when it encountered this "worst case" environment, exceed measured eclipse potentials.

Different spacecraft charge to different levels in the same environment depending on their surface materials, size, shape, and orientation to the sun. Therefore, absolute charging levels experienced on a particular satellite cannot be accurately compared to absolute charging levels on a satellite of different design. However, if an environment maximizes the relative charging on a space vehicle, then that environment may truly be a "worst case" environment. Below we present an example of such a charging environment as encountered by SCATHA on 24 April 1979. Comments are made on the environmental conditions and regimes where the highest level spacecraft charging can be expected.

To orient those unfamiliar with the SCATHA satellite, we briefly describe the satellite and instrumentation. Geophysical conditions on the charging day are also discussed. The satellite plasma environment is described in the terms of time and pitch angle variations of particle fluxes in different energy ranges and in terms of magnetic field variations. Parameters that are related to satellite charging are identified and correlated. Finally, the particle measurements are represented in forms more suitable for modelling spacecraft charging and discussed in terms of their accuracy in reproducing the ambient plasma features. This should allow each reader to adapt the results to his particular needs.

2. SATELLITE DESCRIPTION AND INSTRUMENTATION

The P78-2 SCATHA satellite was launched into a near-geosynchronous orbit in January 1979. The satellite is cylindrical in shape (~ 1.75m in length and diameter) and has seven experimental booms. The satellite is spin stabilized at approximately 1 rpm with the spin axis of the satellite in its orbital plane and normal to the Earth-Sun line. This allows an outward pointing detector on the cylindrical surface to sample nearly all pitch angles. The satellite is in a 5.5 R_E × 7.7 R_E (R_E = 1 Earth radius), low inclination (~ 8°) orbit, and drifts eastward at about 6° per day. For a more detailed review of the satellite and its instrumentation, see Stevens and Vampola. [1]

Of the thirteen separate experimental payloads aboard the SCATHA satellite, data from seven of the payloads are used in this report. Since the seven experiments are well documented by Stevens and Vampola, [1] only a short description of

1. Stevens, J. R., and Vampola, A. L. (Editors) (1978) Description of the Space Test Program P78-2 Spacecraft and Payloads, SAMSO-TR-78-24.

the three payloads most critical to this study is given here. These experiments are the AFGL Rapid Scan Particle Detector (SC5), the UCSD Charged Particle Experiment (SC9), and the NASA Goddard Electric Field Detector (SC10).

The SC5 detector is comprised of two sets of spectrometers which allow a determination of the ion differential flux from ~100 eV to several MeV and the electron differential flux from ~100 eV to 1 MeV. One set of spectrometers is parallel to the spin axis and measures energetic particles at a nearly constant pitch angle. The other set of spectrometers is perpendicular to the spin axis and sweeps through nearly all pitch angles once per spin. The instrument energy detection ranges and channel widths are listed in Table 1. Data for each energy range are obtained once per second; thus, this instrument provides very fast time resolution with rather broad energy resolution. Its pitch angle resolution is excellent for determining directions and anisotropies in particle flows to the satellite. A summary description and calibration of the instrument are given in Hanser et al.[2]

Table 1. Summary of SC5 Energy Detector Properties

Electrons				Ions	
E(keV)	Δ E(keV)	Sensor	Channel	E(keV)	Δ E(keV)
0.112	0.138	ESA ∥	L.E. 1	0.145	0.134
0.27	0.30		2	0.35	0.34
0.68	0.87		3	0.78	0.79
1.50	1.55		4	1.70	1.57
4.6	6.2		H.E. 1	4.5	4.3
9.0	8.9		2	10.4	8.1
23.0	25.0		3	25.0	20.0
53.0	53.0		4	60.0	47.0
0.110	0.160	ESA ⊥	L.E. 1	0.148	0.148
0.26	0.33		2	0.34	0.33
0.62	0.78		3	0.84	0.86
1.57	1.64		4	1.80	1.62
4.4	5.7		H.E. 1	4.0	3.9
9.2	9.1		2	9.7	7.8
24.0	26.0		3	23.0	19.0
54.0	55.0		4	55.0	45.0
		SSS ∥ and ⊥	A 0	126	49
			1	188	75
96	48		2	275	100
335	430		3	388	125
218	95		4		

A - Anticoincidence
SSS - Solid State Spectrometer
ESA - Electrostatic Analyzer
L.E. - Low Energy
H.E. - High Energy

2. Hanser, F.A., Hardy, D.A., and Sellers, B. (1979) Calibration of the Rapid Scan Particle Detector Mounted in the SCATHA Satellite, AFGL-TR-79-0167, AD A082382.

The SC9 experiment consists of five electrostatic analyzers. Four of the detectors (two that detect negative particles and two that detect positive particles) can be rotated while one positive particle detector is fixed with respect to the vehicle spin axis. The high energy detectors sample the energy range from ~1 eV to 80 keV in 64 discrete energy steps, and the low energy detectors sample the energy range from ~1 eV to 2 keV in 64 discrete steps. The energy steps are exponentially spaced. The scan rate for all 64 energy channels is once per 16 seconds. Because the energy resolution is much better than the SC5 instrument, the SC9 data are used here primarily to determine vehicle frame to ambient plasma potentials (ϕ_f) for values greater than 1 kV. The method of using particle data to determine vehicle charging is identical to that developed by DeForest.[3] A complete explanation of the SC9 Charged Particle Experiment and its energy resolution is contained in an unpublished UCSD Handbook dated 1978.[4]

The SC10 detector consists of two 50-m antennas that form a 100-m dipole. The inner 30 m of each antenna is coated with Kapton insulation so that the outer 20-m conducting surfaces act as a double floating probe ensemble to measure dc electric fields in the ambient plasma. Also, a measurement of the voltage difference between one of the antennas and spacecraft ground provides high time resolution (twice per second) measurements of ϕ_f below 500 V. Above $\phi_f \approx 500$ V, probe charging and/or satellite plasma sheath effects contaminate the measurements. The SC10 data are used here primarily as a high time resolution sunlight vehicle charging monitor.

3. "WORST CASE" SPACECRAFT CHARGING LEVEL

The "worst case" spacecraft charging levels occurred on SCATHA on 24 April 1979 between 0635 and 0730 UT. For this period, the satellite varied in distance from the center of the Earth between 6.45-6.75 R_E (passing through geosynchronous orbit), in L-shell from 7.0-7.3, and in magnetic latitude from 0.7°-1.2°N. At ~0635 UT (~2300 Local Time), while still in sunlight, ϕ_f began to increase. It increased steadily (in the negative sense) from several volts to several hundred volts until a maximum sunlight value of -340 V was reached between 0651 and 0653 UT. Over the next 20 min, the satellite potential had large variations but remained charged above the ~ -50 V level until the satellite entered eclipse at 0710 UT. In eclipse, the satellite potential reached a maximum value greater than -8 kV and

3. DeForest, S.E. (1972) Spacecraft charging at synchronous orbit, JGR, 77:651-659.

4. UCSD Space Physics Lab Staff (1978) Handbook for UCSD SC9 SCATHA Auroral Particles Experiment, Unpublished.

remained at potentials greater than -1 kV throughout the eclipse period. Upon reentering sunlight at 0805 UT, ϕ_f dropped to less than -50 V and returned to an uncharged state by 0850 UT. A summary plot of the satellite potential as a function of time is given in Figure 1 for values of ϕ_f greater than -100 V. In sunlight, the potential values are those of SC10 taken once per spin at the same sun angle; in eclipse, the values are derived from the SC9 ion charging peak. The gaps in the data are for time intervals during beam operations.

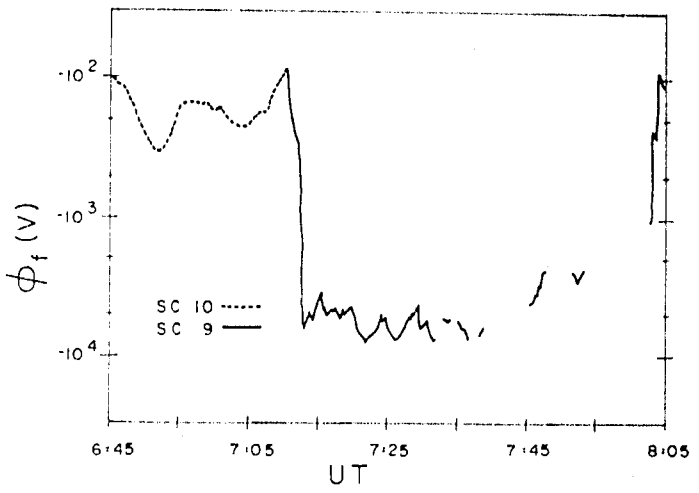

Figure 1. SCATHA Vehicle Frame Charging (ϕ_f) Greater Than -100 V as Measured by SC10 in Sunlight and SC9 in Eclipse Between 0645 and 0805 UT 24 April 1979

While the eclipse condition resulted in an increase of the satellite potential by nearly two orders of magnitude, the worst environment for spacecraft charging actually occurred during the period of sunlight charging. Evidence for this is given below. In fact, the -340 V charging peak represents one of the highest levels of SCATHA sunlight charging observed during the first year of operation. The satellite potential, as measured by SC10, for the sunlight charging period (0635-0710 UT) is shown in greater detail in Figure 2. Here, every point (one every 0.5 sec) is plotted, except for those times when the SC10 boom was pointing nearly directly at the sun or was in the vehicle shadow. At these times, boom charging effects contaminate the data. The high time resolution of the SC10 measurement clearly shows a spin cycle variation in the satellite potential superimposed on a more slowly varying response to environmental changes. Figure 3 is an expansion of the potential plot for three spin-cycles, from 0655 to 0658 UT. The spin-cycle variation is

nearly 80 V and is extremely regular. It is due to rotation of various satellite surface materials with different photoelectron emissivity properties in and out of sunlight. To determine temporal variations in ϕ_f independent of material properties, sun angle, and so on, we represent ϕ_f by its maximum value for each spin. This value occurred each spin at the same satellite-sun orientation.

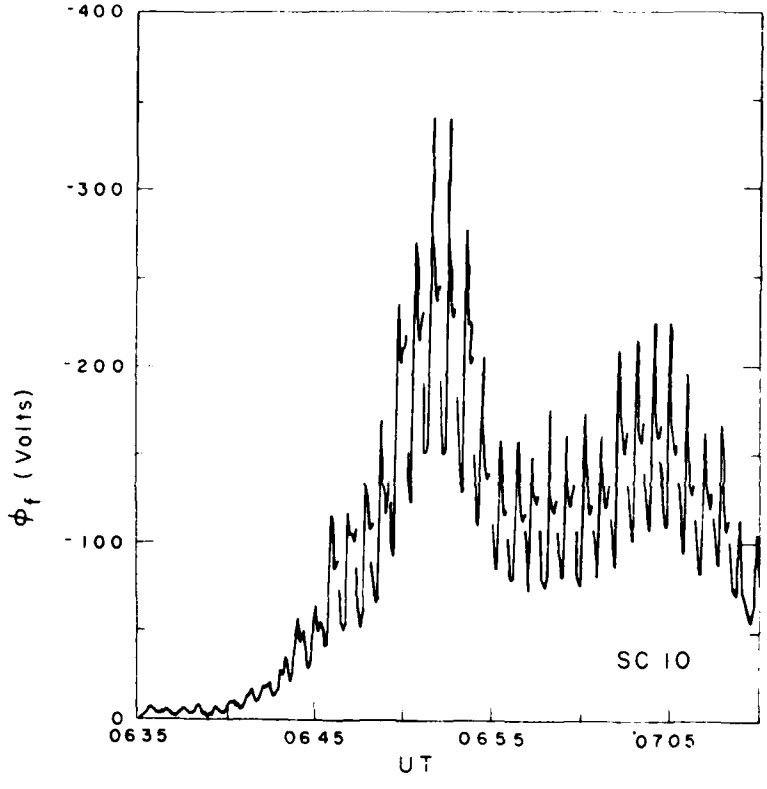

Figure 2. Vehicle Frame Charging (ϕ_f) Measured by SC10 at 0.5 sec Resolution for the Pre-eclipse Period

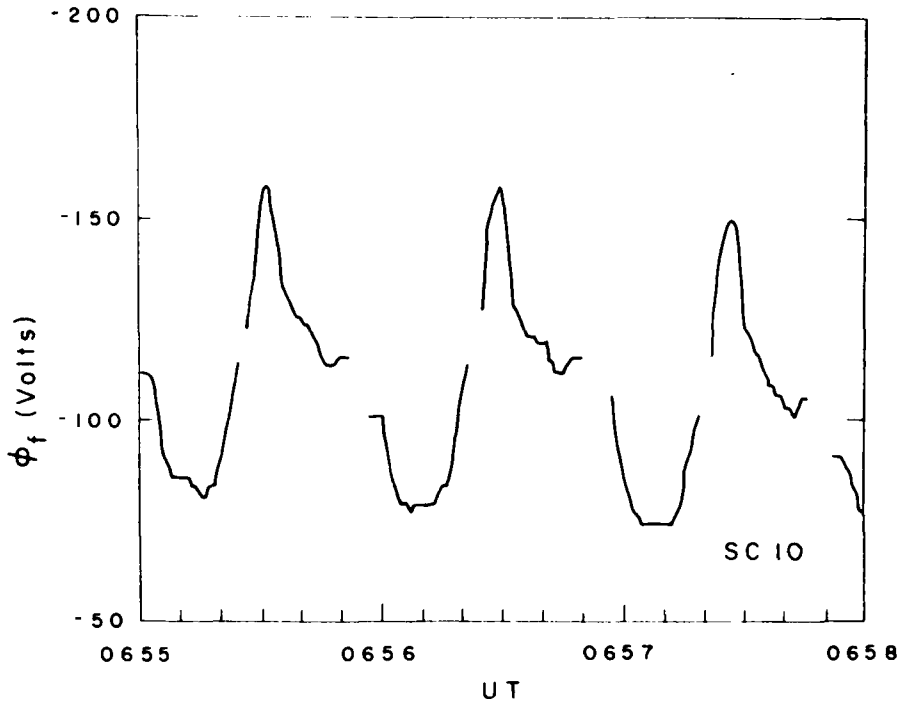

Figure 3. Vehicle Frame Charging (ϕ_f) Measured by SC10 at 0.5 sec Resolution in an Expanded Time Scale Showing Spin/Sun Angle Effects

For completeness, surface material charging data from the SC1 Aerospace Satellite Surface Potential Monitors (SSPM's) provided by P. F. Mizera are shown in Figure 4. The plots show the highest charging levels reached by the various materials in 1-min intervals. The plots terminate at 0655 UT due to a power-down of the instrument at that time. Data were not available again from SC1 until after eclipse. Certain material samples, such as the quartz fabric and silvered teflon, charged to their highest level in the first year of operations at this time. Additional information on the SSPM's, their operation, and data for this event are available in References 5 and 6.

5. Mizera, P. F., Leung, M. S., and Kan, H. K. A. (1980) Laboratory and Space Results From the SSPM Experiment, Aerospace Report No. TOR-0080(5505-02)-2.

6. Mizera, P. F., Koons, H. C., Schnauss, E. R., Croley, D. R., Jr., Kan, H. K. A., Leung, M. S., Stevens, N. J., Berkopec, F., Staskus, J., Lehn, W. L., and Nanewicz, J. E. (1981) First Results of Material Charging in the Space Environment, Aerospace Report No. TOR-0081(6506-01)-1.

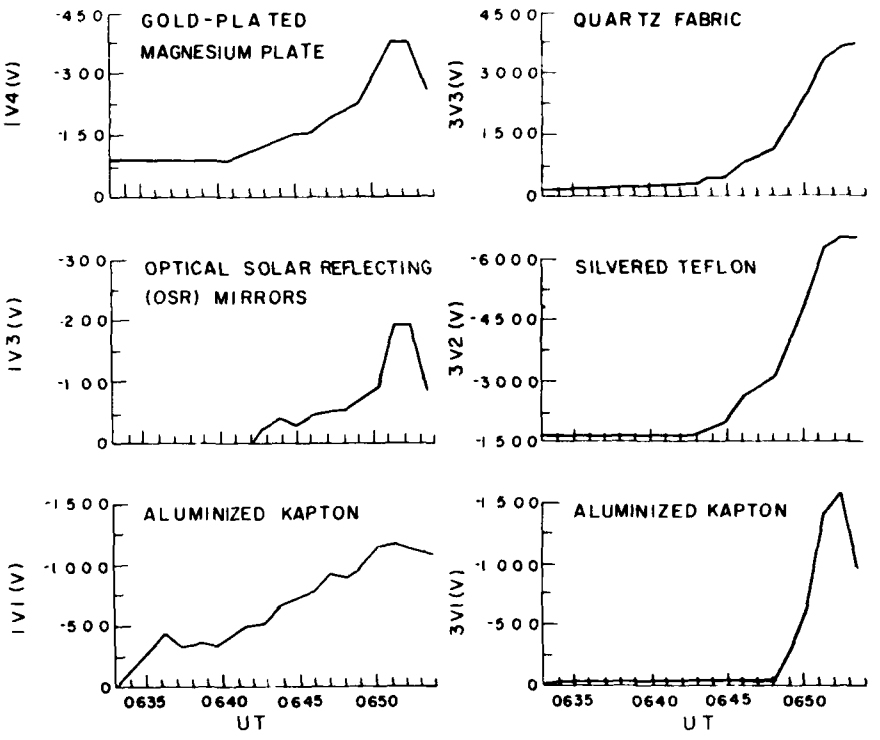

Figure 4. Maximum SSPM Surface Charging Levels in 1-min Intervals Plotted vs UT for Pre-eclipse Charging

4. MAGNETOSPHERIC CONDITIONS FOR "WORST CASE" EVENT

Two methods of specifying the satellite environment are used here. The first is to specify the overall state of the magnetosphere by means of magnetic indices, giving a history of the storm and substorm activity in which the events occurred. Overall conditions provide a framework in which to understand driving mechanisms for local time variations. The second is to specify the plasma as measured on the satellite. Full specification of the plasma requires knowledge of the magnetic field, the electric field, the particle population, and the time variations of each of these. The ambient electric field cannot be specified during charging events since it is two to three orders of magnitude less than the electric fields built up around the satellite. In addition, as mentioned above, the low energy particle measurements (particles with energies near and less than ϕ_f) were also affected during charging.

4.1 Ground Magnetic Indices

Figure 5 shows the magnetic activity indices, K_p, Dst, and AE for the period 21-24 April 1979. A provisional AE index was compiled by Meng[7] using only Alaskan, Canadian, and U.S. stations. On 21 April, activity levels for K_p, Dst, and AE all increased from previously low values. The ring current magnitude, measured by Dst, and the mid-latitude magnetic activity, K_p, grew in a gradual and storm-like fashion, reaching maximum values at the beginning of 22 April, after which both slowly decayed for the following three days. Auroral activity, measured by AE, increased abruptly on 21 April, and continued at high values (up to ~800 nT) into 23 April, indicating the occurrence of multiple substorms. The worst case charging event, (marked by a dot in Figure 5) occurred during an isolated substorm that took place from 0645 UT to 0800 UT, as the overall magnetic activity subsided.

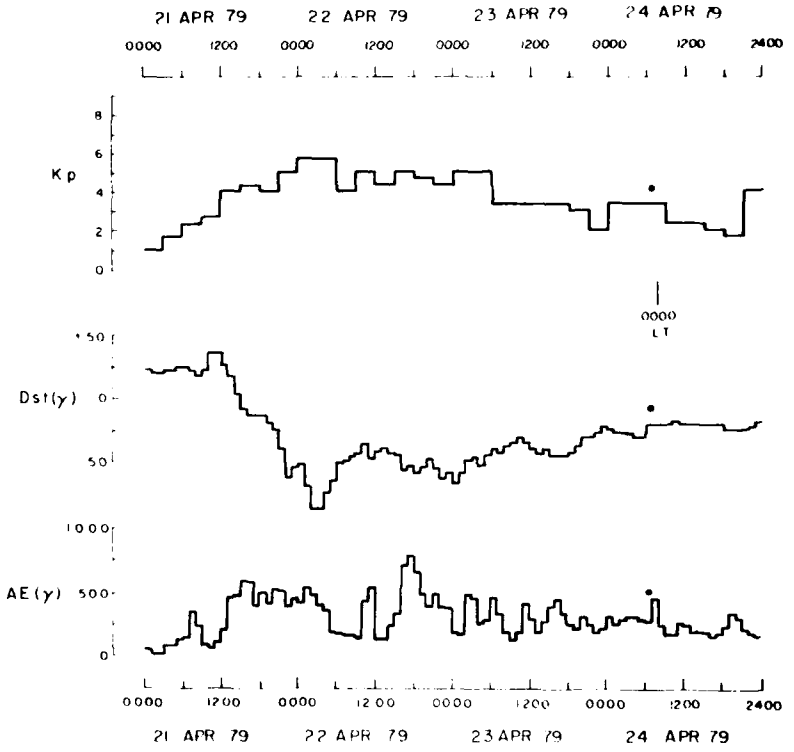

Figure 5. Geomagnetic Indices K_p, Dst, and AE for the Time Period From 21 April 1979 Through 24 April 1979. The dot denotes the "worst case" charging event time

7. Meng, C. -I. (1979) The Investigation of the Magnetospheric Dynamics in Conjunction With the SCATHA Satellite Observations, AFGL-TR-80-0070, AD A087433.

4.2 Magnetospheric Magnetic Field

Onboard SCATHA the magnetic field as measured by the SC11 NASA Goddard magnetometer[8] shows the following variations in solar magnetic coordinates when compared to the quiet magnetic field model of Olson and Pfitzer.[9] For ~24 hours prior to 0600 UT on 21 April, the measured and model fields were nearly identical. At ~0600 UT (2100 MLT) on 21 April, a gradual decrease in B_z of ~30 nT took place over 1 hour. The B_x and B_y components varied only slightly during this time. This type of variation from the model, dipole-like field, represents a more tail-like configuration. The field remained moderately disturbed and tail-like through 1200 UT on 22 April, when it returned to the model field. A smaller, tail-like excursion from the model field occurred at ~1600 UT on 22 April and persisted with variations to 0645 UT on 24 April. At this time approximate values for the measured (model) field components were: B_x = 7(5) nT; B_y = -12(-3) nT; B_z = 70(90) nT. By 0655 UT on 24 April, the magnetic field had dynamically returned to a near model field configuration. The variations in B_z from 0635-0710 UT on 24 April are shown in detail in Section 5.

4.3 Particle Populations

Figure 6 is a spectrogram from the SC2 Aerospace particle detector of electron (top panel) and ion (bottom panel) fluxes for 24 April, from 0000-1200 UT.[10] The SC2 detectors were turned off for active experiments just prior to 0730 UT. At ~0330 UT (~1900 MLT) the SCATHA satellite entered the plasma sheet. At this time the spectrogram showed a sharp increase in low energy electrons. As the satellite moved to higher altitudes, it crossed more energetic Alfven layers (boundaries of higher energy electrons). This dispersion in electron fluxes which is characteristic of a quiet plasma sheet crossing[11] continued for several hours. At ~0630 UT, the satellite was well within the plasma sheet, having crossed the 20 keV Alfven layer. A major change occurred in the electron spectrogram at ~0615 UT with sharp decreases in electron fluxes for energies less than 1 keV.

---

8. Ledley, B.G., Private communication.
9. Olson, W.P., and Pfitzer, K.A. (1974) A quantitative model of the magnetospheric magnetic field, JGR, 79:3739-3748.
10. Fennell, J.F., Private communication.
11. Kivelson, M.G., Kaye, S.M., and Southwood, D.J. (1979) The physics of plasma injection events, in Dynamics of the Magnetosphere, edited by S.I. Akasofu, 385-394, D. Reidel, Hingham, Massachusetts.

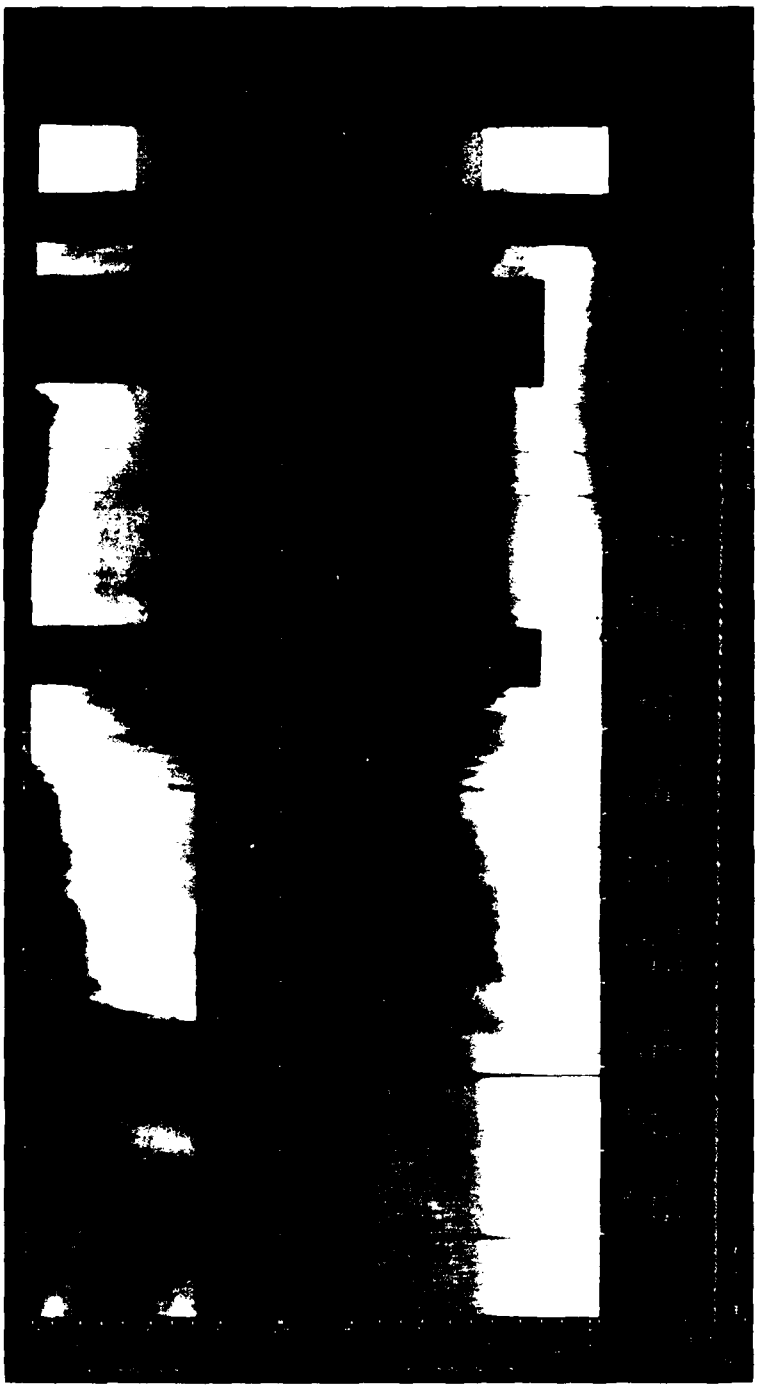

Figure 6. SC2 Spectrogram of Ion and Electron Energy Flux vs Energy and UT for the First 12 Hours of 24 April 1979

The particle fluxes are shown in greater detail in Figure 7. Here SC5 data are used to extend the plasma description to higher energies. The lefthand side of Figure 7 gives the electron fluxes for energies from 620 eV to 335 keV; the right-hand side gives ion fluxes for energies from 4 keV to 388 keV. The fluxes are plotted in linear scales. The solid lines represent measurements made perpendicular to the magnetic field. The dotted lines are for measurements made at pitch angles nearest to 180° (anti-parallel to the magnetic field). For the period of interest, the closest approach to the field was ~15°. The crossings of Alfven layers for the 9 keV and 23 keV energy channels were at 0605 UT and 0635 UT respectively. Lower energy crossings occurred prior to 0530 UT. The fluxes are preferentially aligned perpendicular to the magnetic field indicating well-developed loss cones; a characteristic of the quiet plasma sheet.

After 0600 UT, perpendicular electrons with energies less than 5 keV began to decrease, approaching the flux levels of the parallel electrons. By 0635 UT, the lower energy particle population was nearly isotropic and remained this way through to 0900 UT.

At ~0645 UT the perpendicular electron fluxes in all the high energy channels, down to and including the 23 keV channel increased sharply. This was followed by a second, larger increase that peaked near 0651 UT. The increases occurred only in the perpendicular electrons resulting in a more anisotropic hot component in the plasma. This dynamic injection in the highest energy channels is associated with the SCATHA "worst case" charging event and the isolated substorm seen in ground magnetic variations. After the injection peak, the electron fluxes and average energy decreased (with fluctuations) until 0900 UT, at which time the total electron environment was nearly isotropic.

The ions over the energy range from ~4 keV to 388 keV are shown in the right-hand side of Figure 7. This figure shows that: (a) the > 100 keV perpendicular ion fluxes had the same large scale increase near 0650 UT that the electrons had: (b) the 23.1 keV perpendicular ions decreased markedly during the peak of the electron injection event after 0650; (c) the ions accelerated to the vehicle during high level charging in eclipse (0710-0800 UT) were preferentially field aligned; and (d) although the lower energy ions were more isotropic over the entire period than their electron counterparts, the > 100 keV ions behaved in the same way as the high energy electrons. Ion mass data provided from the SC8 Lockheed ion mass spectrometer[12] give evidence for field aligned streaming of O^+ during high level charging periods. The average density ratio $n(O^+)/n(H^+)$ over the energy range measured (0.2 - 32.0 keV) was 0.41 ± 0.10 for the sunlight charging period.

---

12. Johnson, R.G., Private communication.

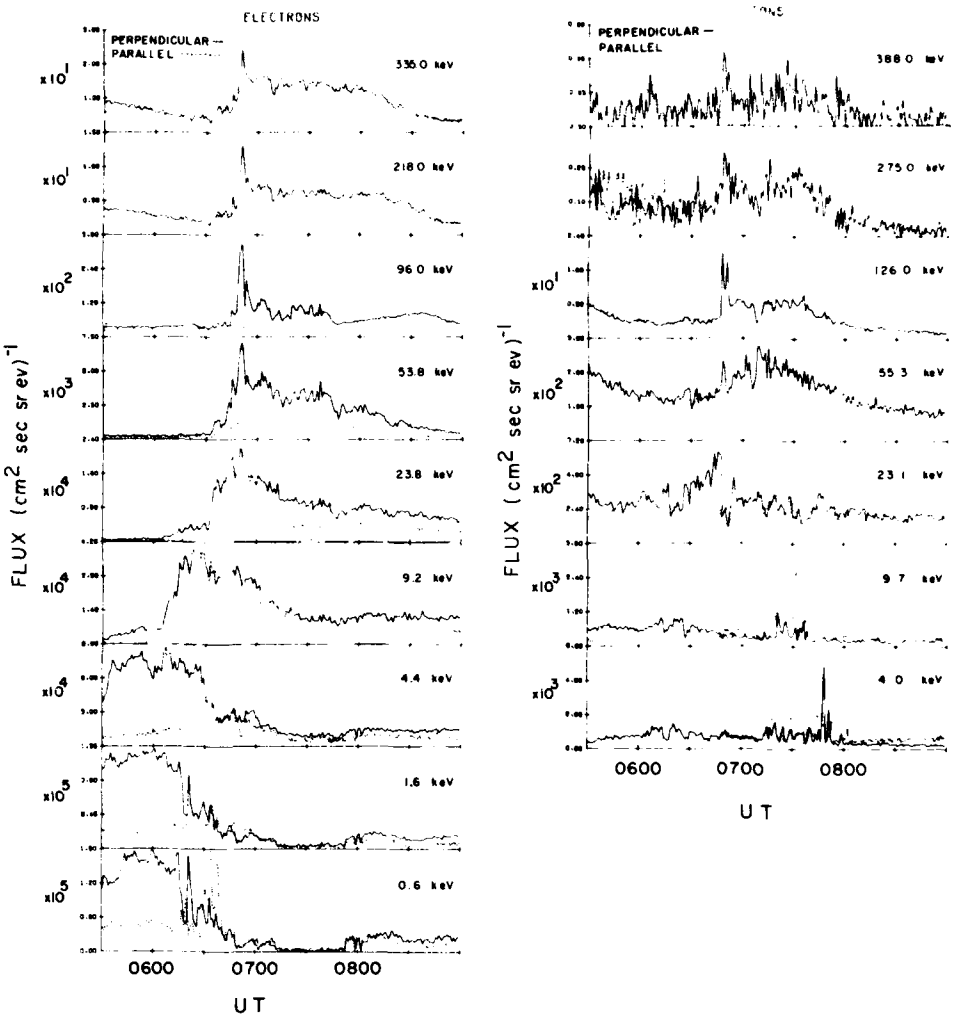

Figure 7. SC5 Electron (left) and Ion (right) Fluxes as Measured Perpendicular (solid line) and at ~165° (dashed line) to the Magnetic Field Over the Energy Range 0.6 keV to 335 keV for Electrons and 4 keV to 388 keV for Ions Plotted vs UT on 24 April 1979

SC5 measurements of ion fluxes for the energy range 50 eV - 2 keV (not shown in Figure 7) reach values above background only sporadically, last only 1-3 sec, and fluctuate greatly. No significant changes in these fluxes are discernible from the pre-charging through the sunlight-charging period. Ion counts in the SC2 detectors for the energy range 74-360 eV are low prior to sunlight charging and show weak field alignment. During sunlight-charging, low intensity, field aligned

charging peaks can frequently, but not always, be identified. We conclude from these measurements that the low energy (< 1 keV) ion population was very small during the charging event. On 24 April, GEOS 2, in synchronous orbit and with the capability of measuring the cold ion population, lagged SCATHA by ~ 12 hours in local time. No significant cold ion population (< 1 cm^{-3} was measured on either 23 or 24 April in the midnight sector (2100-0300 MLT).[13]

The characteristics of the magnetospheric plasma for the "worst case" charging on SCATHA are summarized by the spectra in Figure 8. The ion and electron distribution functions (in km^{-6} sec^{3}) for measurements made perpendicular to the magnetic field are shown for the highest sunlight-charging level at ~0650 UT (solid line) and (for reference) for the pre-charging time at 0630 UT (dashed line).

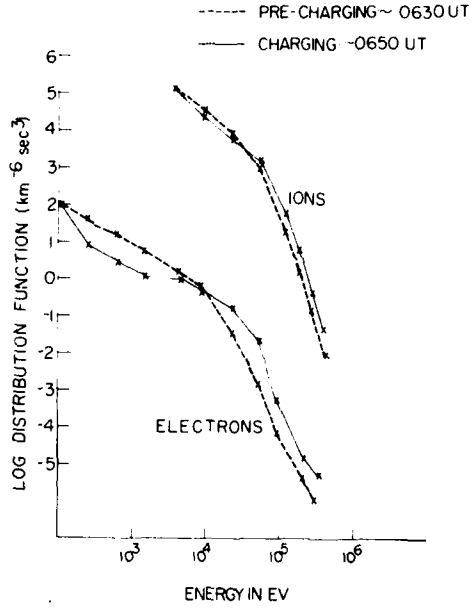

Figure 8. Ion and Electron Distribution Functions for Pre-charging Environment at ~0630 UT and a Charging Environment at ~0650 UT Plotted vs Particle Energy on 24 April 1979

The ion and electron spectra both deviate from the pre-charging spectra in the same manner; a decrease in phase space density for lower energies and an increase for higher energies. The energy at which no change occurs is 10 keV for electrons and 30 keV for ions. The electron distribution function variations are greater than those for ions. We note here that although the pre-charging spectra are used for

13. Gordon Wrenn, Mullard, UCL, Private communication.

reference, they, themselves are considerably harder than those frequently found in the plasma sheet.

5. DATA ANALYSIS

In the previous section evidence was presented which indicates that the "worst case" environment occurred during the injection of high energy (> ~30 keV) electrons perpendicular to the magnetic field and a simultaneous depletion of lower energy electrons (between ~ 1-10 keV; at energies greater than those strongly affected by the sunlight satellite potential). The environment was also characterized by the absence of a significant ($\leq$ 1 cm^{-3}) cold- to low-energy ion population. In this section, a staistical data analysis shows that strong interrelationships exist among ϕ_f, high energy electron fluxes, and magnetic field behavior. In addition, we calculate the particle number densities, temperatures, and distribution functions during charging. Together these studies present a picture of the high level charging environment.

5.1 Correlation Analysis

Figure 9 shows in detail geophysical parameters whose variations are similar to the variations in ϕ_f. The left-hand side of Figure 9 is for sunlight conditions, the right-hand side for eclipse conditions. The bottom panel gives ϕ_f. In sunlight, the values of ϕ_f are obtained from SC10, taking the maximum value per spin. In eclipse, the values of ϕ_f are determined from the SC9 ion charging peak. The second panel is the z-component of the magnetospheric magnetic field in solar magnetic coordinates as measured by SC11. Also shown (dashed line) is the z-component of the model magnetospheric field of Olson and Pfitzer.[9] The top two panels are electron fluxes for two energy ranges measured by SC5 and plotted once per spin when the detector was perpendicular to the magnetic field. The average energies for the two ranges are 53.8 keV and 96.0 keV. All variables are plotted linearly.

To make a quantitative assessment of the relationship between electron fluxes and ϕ_f, linear regressions between the two were performed for each energy channel above the charging peak. In sunlight, the regressions were performed for the period 0635-0710 UT. For each energy channel 37 pairs of points were used; one pair per spin. The resulting correlation coefficients (r's) are given in Table 2. A Student's t test of the significance level of the coefficients showed that they are highly significant (exceeded the 0.1% level) for all channels including and above the 53.8-keV channel. The correlation coefficient drops sharply from 0.94 to 0.42 between the 53.8-keV channel and the 23.8-keV channel. It reverses sign and remains low for the 9.2-keV and 4.4-keV channels. For the two lowest channels, 1.57 keV and 0.62 keV, there is a high anti-correlation between the fluxes and ϕ_f.

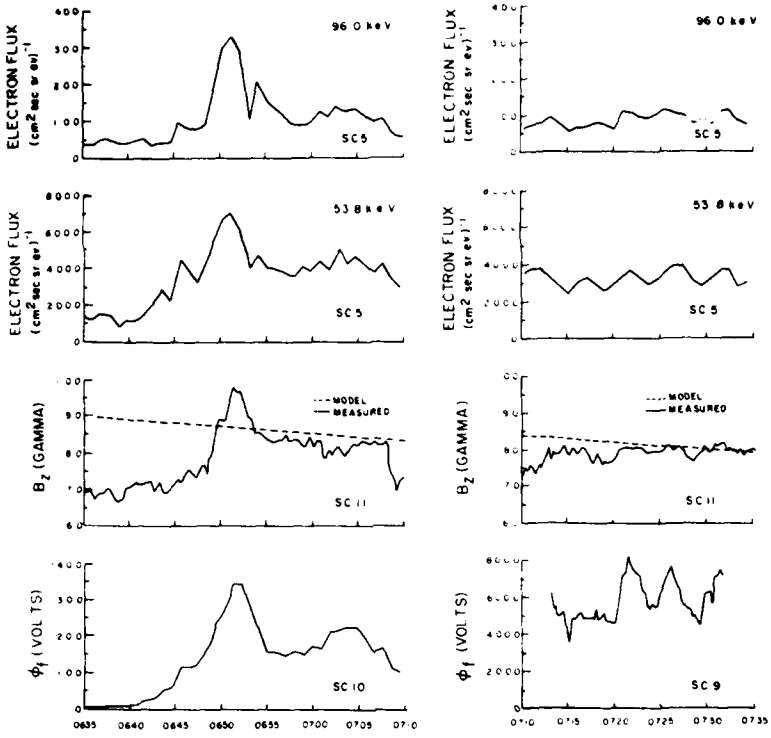

Figure 9. A Time History of Vehicle Frame Charging Both Before (left) and During (right) Eclipse Together With Associated Geophysical Parameters Between 0635 and 0735 on 24 April 1979. The top two panels show SC5 electron fluxes measured at 96 keV and 53.8 keV respectively. The third panel shows the B_z component of the magnetic field in SM coordinates as measured by SC11 (solid line) and the Olson and Pfitzer quiet model for the same interval (dashed line). The bottom panel shows ϕ_f as measured by SC10 (left) pre-eclipse and SC9 (right) in eclipse

In eclipse, the linear regressions were performed for the period 0713-0730 UT when the vehicle potential varied between 3.6 and 8.2 keV (Figure 9). Although the flux levels are lower than the peak flux levels during the sunlight-charging period, they also have considerable variation. The correlation coefficients, (r's), between ϕ_f and the perpendicular electron fluxes for energies above 8 keV are given in Table 3.

Table 2. Correlation Coefficients of φ_f vs Electron Flux in Sunlight

SC5 Energy Bin (keV)	r
0.62	-0.87
1.57	-0.72
4.4	-0.28
9.2	-0.36
23.8	+0.42
53.8	+0.94
96	+0.85
218	+0.92
335	+0.92

Table 3. Correlation Coefficients of φ_f vs Electron Flux in Eclipse

SC5 Energy Bin (keV)	r
9.2	-0.59
23.8	-0.31
53.8	+0.79
96	+0.88
218	+0.51
335	+0.71

Here 20 pairs of points were used for each regression. A Student's t test of the significance level of the coefficients showed that the 53.8, 96, and 335 keV electron flux coefficients are highly significant (exceeded the 0.1% level) and the 218-keV flux coefficient is significant (exceeded the 1% level).

Because both the sunlight- and the eclipse-charging are highly correlated with the high energy (greater than ~ 30 keV) fluxes, we conclude that it is the high energy tail of the electron spectrum that is primarily responsible for high-level satellite charging. The high correlation coefficients also permit extrapolation of the fluxes in sunlight on 24 April 1979 to give eclipse values for φ_f. To do this the assumption must be made that the low-energy component (electron and ion) of the plasma remained approximately constant from 0635 to 0730 UT. The assumption is reasonable since the satellite remained in the plasma sheet for the entire period and there was no significant cold ion population (see Section 4). Extrapolating ϕ_f to eclipse conditions using linear regression equations for both the 96-keV and the 53.8-keV electron fluxes gives values of 18 kV and 15 kV respectively at 0651 UT. Both values are higher than any known charging level seen to date on the SCATHA satellite.

The B_z component of the magnetic field is also seen to vary considerably over the period 0630 to 0730 UT. The largest variations were between 0648 and 0653 UT.

simultaneous with the injection events (Figure 9). B_z was found to highly correlate with both the SC10 charging levels prior to eclipse ($r = 0.93$) and the 53.8-keV electron fluxes ($r = 0.90$) through the entire period. This interrelationship among B_z, ϕ_f, and high-energy electron flux provides insight into physical mechanisms that occur in the plasma sheet during high-level charging events. Although a complete description of the mechanisms is both unknown and beyond the scope of this report, some of the magnetospheric characteristics during high level charging will be discussed later.

5.2 Moments of the Distribution Function

Certain properties of the plasma can be calculated by taking various velocity moments of the ion and electron distribution functions constructed from particle measurements. For SC5, the first four moments (zero-order through third-order) are related to number densities and fluxes of a given particle species as follows:

Number density, n: $$\int f\, d^3v \ (cm^{-3}), \tag{1}$$

Number flux, NF: $$\int |v|\ f\, d^3v \ (cm^{-2}\text{-}s^{-1}) \tag{2}$$

Energy density, ϵ: $$1/2\ m \int v^2\ f\, d^3v \ (eV\text{-}cm^{-3}), \tag{3}$$

Energy flux, EF: $$1/2\ m \int |v^3|\ f\, d^3v \ (eV\text{-}cm^{-2}\text{-}s^{-1}). \tag{4}$$

In these equations, f and m are the distribution function and mass for a given particle species and the integration is taken over the entire velocity space. For the SC5 measurements, symmetry is assumed in the plasma perpendicular to the magnetic field and integrations are performed over pitch angle and v. The fluxes (number and energy) in Eqs. (2) and (4) are the total fluxes that would be intercepted by an infinitesimally small, omni-directional receiving device. In practice directional fluxes ($cm^{-2}\text{-}s^{-1}\text{-}sr^{-1}$) are often used (no integration in angular space). In order to incorporate pitch angle information, average directional fluxes can be calculated from Eqs. (2) and (4) by multiplying by $1/4\pi$.

From the first four moments there are two ways of defining temperature:

1) $$T_{AVG} = \frac{2}{3} \cdot \frac{n}{\epsilon}, \tag{5}$$

and

2) $$T_{RMS} = \frac{1}{2} \cdot \frac{EF}{NF}. \tag{6}$$

For a distribution function that is well fit by the Maxwell-Boltzmann function:

$$f(v) = n\left(\frac{m}{2\pi kT}\right)^{3/2} e^{-mv^2/2kT}, \tag{7}$$

the two temperatures are equal; that is,

$$T = T_{RMS} = T_{AVE}. \tag{8}$$

(In Eq. (7), k is the Boltzmann constant = 1.38×10^{-16} erg/°K.) In general, however, distribution functions are not Maxwellian over the entire energy range and the concept of temperature is an ambiguous one.

Table 4 gives the first four moments of the ion and electron distribution functions, together with T_{AVE} and T_{RMS}, during the "worst case" charging at ~0650 UT on 24 April. The SC5 measurements over the energy range 100 eV-400 keV were used to construct the distribution functions. Integrations over pitch angle were used for all moments; therefore, the number and energy flux are average directional quantities. The moments for ions were calculated assuming hydrogen as the only species. Johnson[12] has provided composition data in the 0.2- to 32-keV energy range that show that the average density ratio $n(O^+)/n(H^+)$ is between ~0.3 and 0.5 over the daylight charging period. This would have the effect of raising the ion number density and energy density roughly by a factor of 2. The temperatures and fluxes would remain about the same. Care must be taken in interpreting the moment results since the cold population was missing and the low energy end of the spectrum was influenced by ϕ_f.

Table 4. Moments and Temperatures Integrated Over Pitch Angle

	Electrons	Ions
Number Density	0.9 cm^{-3}	2.3 cm^{-3}
Number Flux	4.7×10^9 cm^{-2}-s^{-1}-sr^{-1}	2.0×10^8 cm^{-2}-s^{-1}-sr^{-1}
Energy Density	9.6×10^3 eV-cm^{-3}	1.9×10^4 eV-cm^{-3}
Energy Flux	8.4×10^{13} eV-cm^{-2}-s^{-1}-sr^{-1}	5.4×10^{12} eV-cm^{-2}-s^{-1}-sr^{-1}
T_{AVE}	7.7 keV	550 eV
T_{RMS}	9.0 keV	14 keV

The same moments assuming isotropic particle distributions and using particles fluxes at 90° pitch angle are given in Table 5. The difference between the corresponding quantities in Tables 4 and 5 give a measure of the anisotropy of the plasma.

Table 5. Moments and Temperatures Using $\perp$ Particles Only

	Electrons	Ions
Number Density	1.5 cm^{-3}	1.4 cm^{-3}
Number Flux	9.2×10^{9} cm^{-2}-s^{-1}-sr^{-1}	2.1×10^{8} cm^{-2}-$s^{-1}sr^{-1}$
Energy Density	2.1×10^{4} eV-cm^{-3}	2.4×10^{4} eV-cm^{-3}
Energy Flux	1.94×10^{14} eV-cm^{-2}-$s^{-1}sr^{-1}$	7.2×10^{12} eV-cm^{-2}-$s^{-1}sr^{-1}$
T_{AVE}	10.4 keV	12.6 eV
T_{RMS}	11.3 keV	16.8 keV

The four moments have been used by Garrett,[14] among others, to solve for the number densities and temperatures of a two-Maxwellian representation of the distribution function. The two-Maxwellian representation is an additive one:

$$f(v) = n_1\left(\frac{m}{2\pi kT_1}\right)^{3/2} e^{-mv^2/kT} + n_2\left(\frac{m}{2\pi kT_2}\right)^{3/2} e^{-mv^2/kT_2}, \qquad (9)$$

and requires four quantities for its specification: n_1, n_2, T_1, and T_2. When these quantities are calculated from the four moments, there is no freedom of choice to determine the energy ranges for the high and low temperatures; nor is it possible to assume that the energy ranges remain nearly the same from spectrum to spectrum. In fact, for spectra which are rapidly varying in time, or which are highly non-Maxwellian (as is the case during charging), the high and low components are constantly calculated over different energy ranges. Thus, the time history of a given population (for example, the high-energy electrons) cannot be followed and the results can be misleading.

14. Garrett, H. B. (1977) Modeling of the Geosynchronous Orbit Plasma Environment—Part 1, AFGL-TR-77-0288, AD A053164.

5.3 A Two-Maxwellian Description of the "Worst Case" Environment

The technique of using a double Maxwellian to fit the actual distribution function by no means guarantees the best mathematical fit; however, the double Maxwellian is easy to use (only four numbers are required to define a distribution function) and is conceptually and computationally understood by the engineering community. The one requirement that must be imposed on any representation chosen for the actual distribution function is that it not obscure the physical process it models. The double Maxwellian resulting from the moment techniques did not fulfill this requirement in the "worst case" satellite charging environment; therefore, it will not be used.

Another method of determining double Maxwellian densities and temperatures for a distribution function is by least-squares fitting the logarithm of the distribution function to energy over specific energy ranges. Visual inspection of individual distributions for SC5 data was used to determine an appropriate energy range for calculating the high-energy Maxwellian characterized by n_2 and T_2. The energy range selected for both ions and electrons was 4 keV to 400 keV. The low-energy parameters n_1 and T_1 were calculated by fitting to all the residual data below 4 keV after subtracting extrapolated values from the high energy fit. Figure 10 shows values of the distribution functions for ions and electrons measured by SC5 at ~0650 UT on 24 April. Measurements made both perpendicular and near-parallel to the magnetic field are given. Also shown is the two-Maxwellian representation of each distribution. Solid (dashed) lines represent distributions perpendicular (parallel) to the magnetic field. The low energy Maxwellians (to ~4 keV) must be regarded with caution for the following reasons: (a) the low energy measurements did not extend below 100 eV, (b) the low energy particles were affected by the satellite potential and corrections to the distribution function have not been made for this effect, and (c) the low energy ions were near background and varied sporadically. To create a time varying two-Maxwellian description of the charging period, a method of extrapolating through noisy data was developed which resulted in placing too much weight on values just above background. This is evident in Figure 10 where a low-energy Maxwellian has been included although there is only one good lower energy ion data point at this time.

The high-energy Maxwellians for both ions and electrons, and for both parallel and perpendicular directions to the magnetic field, deviate from the actual distribution functions in two ways, neither of which prevents them from appropriately representing the charging process: First, they underestimate the lower energy spectrum (from ~2-10 keV) which has been shown to relate poorly to satellite charging; and second, they overestimate the values in the energy range (20-200 keV) where direct correlation with charging was found. Thus, in each case the discrepancies

between the Maxwellian fit and the actual spectrum, if anything, place additional emphasis on the particle population that drives satellite charging. The electron and ion densities and temperatures that characterize the double Maxwellians in Figure 10 are listed in Table 6. These represent distribution functions at the time of the sunlight-charging peak.

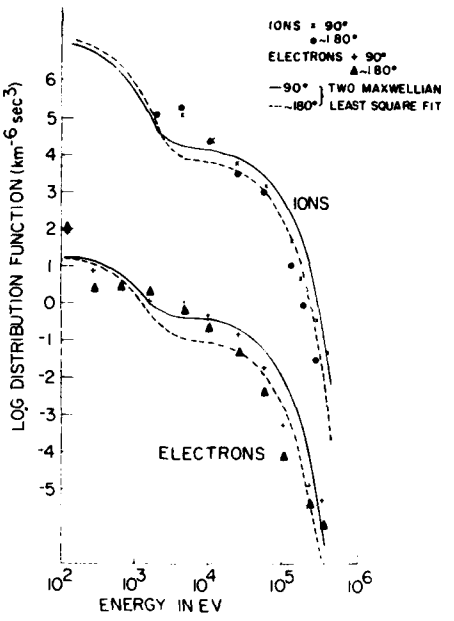

Figure 10. Ion and Electron Distribution Functions Perpendicular and Approximately Antiparallel to the Magnetic Field Together With Their Two-Maxwellian Least Squares Fits for the "Worst Case" Charging Environment on 24 April 1979. (The distribution functions are plotted vs energy from 100 eV to 400 keV

Table 6. "Worst Case" Least-Squares Particle Environment Fit (~0650-UT 24 April 1979)

	n_1 (cm^{-3})	n_2 (cm^{-3})	T_1 (keV)	T_2 (keV)
Ions:				
Perpendicular	1.1	1.3	0.3	28.2
Parallel	1.6	0.6	0.3	26.0
Electrons:				
Perpendicular	0.2	2.3	0.4	24.8
Parallel	0.2	0.6	0.4	24.0

The variations in the four components (n_1, n_2, T_1, and T_2) for electrons with pitch angles ~75° are shown in Figure 11 for the period from 0530 to 0730 UT. T_2, although relatively high, varies only slightly over the entire period. T_1 varies considerably. The high-energy electron density, n_2 rises steadily over the interval from 0530 to ~0651 UT when it peaks. On the other hand, n_1 maximizes near 0614 UT at which time it begins a gradual but variable decline until about 0714 UT. The total electron density (n_1 plus n_2) varies between approximately 1 and 3 particles/cm^3 over the entire period, with n_1 noticeably suppressed due to the high negative vehicle potential after eclipse entry at 0710 UT. (No attempt was made to correct the spectra for charging effects.)

Figure 11 graphically portrays the results of the earlier statistical studies; that is, that the high energy electron current or density is the driver in charging spacecraft to high levels. The decrease (anti-correlation) of n_1 near 0651 UT and the n_2 increase suggest that the low energy particles are being accelerated to higher energies during injection events, and that the introduction of a new higher energy population is not necessarily required. The high- and low-energy ion densities remain nearly constant; each between 1 and 2 particles/cm^3 during the entire period. The high energy ion temperature stays near 28 keV and the low energy temperature near 300 eV. (Again, caution is advised in using the low-energy values.)

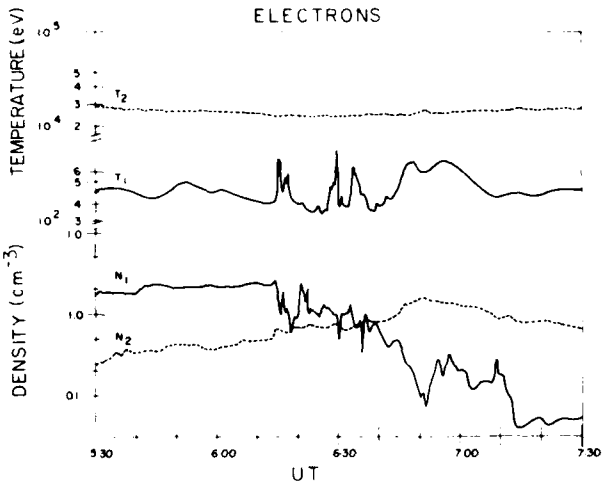

Figure 11. Two-Maxwellian Electron Temperatures T_1 and T_2 and Densities n_1 and n_2 Calculated by Least Squares Fitting the Distribution Functions, Plotted vs UT for the Period From 0530 to 0730 UT 24 April 1979

6. DISCUSSION

Spacecraft charging results from conservation of current to and from a space vehicle. The satellite potential (φ_f) varies until current balance is attained. For a satellite in the magnetospheric environment this relationship may be written:

$$J_E(\varphi_f) - [J_I(\varphi_f) + J_{SE}(\varphi_f) + J_{SI}(\varphi_f) + J_{BSE}(\varphi_f) + J_{PH}(\varphi_f)] = 0 \qquad (10)$$

where

J_E = ambient electron current at the spacecraft surface,
J_I = ambient ion current at the spacecraft surface,
J_{SE} = secondary emitted electron current due to ambient electrons,
J_{SI} = secondary emitted electron current due to ambient ions,
J_{BSE} = backscattered emitted electron current due to ambient electrons,
J_{PH} = photoelectron current.

Here we use the convention that electron currents to the satellite are positive.

At geosynchronous (or near-geosynchronous) orbit a satellite is usually in one of two very different plasma regimes; the plasmasphere or the plasma sheet. The plasmasphere has as its source the ionosphere and is a cold (several eV), dense (~ 10-100 cm^{-3}) plasma that corotates with the earth and extends out from the ionosphere. The outer boundary of the plasmasphere varies greatly with magnetic activity and local time. In quiet periods it can extend beyond geosynchronous orbit, particularly in the dusk and pre-midnight sectors. The outer boundary of the plasmasphere is not always well-defined, and clouds or bursts of cold plasma can extend outward into the neighboring region of the plasma sheet.

Since a cold plasma produces very small ambient currents, the satellite potential in the plasmasphere is dominated by the last term in Eq. (10); the photoelectron current. In the limiting case (that is, the entire cold population has zero energy) no backscattered or secondary particles would be produced and the satellite potential would become positive, inhibiting part of the escaping photoelectron current and accelerating the ambient cold electron population to the satellite. For large densities only small vehicle potentials (on the order of volts) are required to obtain current balance.

The plasma sheet begins where corotation effects are dominated by the magnetospheric electric field. In some local-time sectors the outer boundary of the plasmasphere and the inner boundary of the plasma sheet are identical. In others, they are separated by a region referred to as the trough. The source of the plasma sheet is unclear, although there is evidence that both solar wind and ionospheric

particles are variably involved. Acceleration mechanisms are required to transform both populations into the hot plasmas observed in the plasma sheet. Densities in the plasma sheet are typically of order 1 cm^{-3} and temperatures of the high-energy component typically exceed 10 keV for both ions and electrons. Thus, although the density in the plasma sheet is low, the ambient currents are not. High-level space vehicle charging is limited to periods when the vehicle is in the plasma sheet.

The plasma sheet expands and contracts with solar and magnetic activity. It can reach inward to less than 5.5 R_e during high activity periods. After several magnetically quiet days (days of low K_p) the inner edge of the plasma sheet can be out beyond geosynchronous orbit, in which case no significant spacecraft charging effects would be observed. The boundary of the plasma sheet in local time at geosynchronous orbit can range from ~12 hours around local midnight to none at all. Within the plasma sheet there exist periods when rapid earthward movement of energetic particles is observed. These particle injections appear in the midnight sector in conjunction with geomagnetic substorms and high-latitude auroral activity, and depending on their energy and density, can create satellite charging. The cold (< 1 to 100 eV) particle density in this region is typically low and often less than 1 cm^{-3}. It is this combination of intense high-energy electron fluxes in the near absence of a cold ion population that is responsible for high level spacecraft charging.

Numerous papers have been written that try to explain the mechanism for injection events in the plasma sheet. Here we do not try to develop or justify any model but try only to give a cursory explanation of the data in terms of current thinking. Sauvaud and Winckler[15] give a schematic representation of the geomagnetic field lines during the different phases of a substorm. A substorm, as described in their report, consists of an expansion phase when the magnetic field lines move out and become more tail-like and a collapse phase when the field lines return to a more dipolar configuration. As can be seen in Figure 9, it is during periods when the magnetic field collapses from a more tailward configuration toward a more dipolar configuration that electrons are accelerated to and/or injected at higher energies. These large magnetic field collapses are associated with substorm onsets which can be seen on the ground as AE magnetic index increases (see Figure 5). During substorm collapse, the high energy electron densities can be sufficiently large in certain spatial regimes of the plasma sheet to cause large current imbalance to satellites in the same regime. Numerous substorms take

15. Sauvaud, J. -A., and Winckler, J. R. (1980) Dynamics of plasma energetic particles, and fields near synchronous orbit in the nighttime sector during magnetospheric substorms, JGR, 85:2043-2056.

place which would severely charge space vehicles if the spacecraft were: (a) in eclipse, (b) in the plasma sheet with large high energy (> ~30 keV) electron density, (c) in a plasma sheet with little or no cold plasma population, and (d) oriented in such a way that large areas were exposed perpendicular to the magnetic field. Although the eclipse case is the extreme for frame charging, it is not necessarily the extreme for differential charging. Luckily, however, the probability of a satellite being at the right place at the right time under the right conditions to experience a "worst case" environment is quite small. Also, the exact position in local time where the injection front first reaches geosynchronous altitude is not clear. The case considered for SCATHA was a plasma sheet pre-midnight period, as was the worst case ATS-6 sunlight-charging event.[16] Further statistical studies of the SCATHA data base should provide insight into locating this region.

The environment observed at ~0650 UT on 24 April 1979, and called here a "worst case" environment occurred in an injection event associated with an isolated substorm observed in ground magnetograms after a long active period (multiple substorms). The electron fluxes associated with charging as shown in Figure 7 were very anisotropic with the highest fluxes being perpendicular to the field lines. As was also determined in Tables 2 and 3 and shown in Figure 9, the particles that directly correlate with ϕ_f are the particles in the 53.8-keV energy range and above. Summing the currents in the 53.8-keV through 335-keV energy channels and performing a linear regression with φ_f, gives a correlation coefficient of 0.95. This indicates that it is the total current for energies above ~30 keV (given the ΔE of the 53.8-keV channel) that is driving ϕ_f negative (see, for example, Garrett et al[17]). The lower energy fluxes (and currents), although larger, evidently produce enough backscatter and secondary electrons to balance themselves minus the photoelectron current. Evidence for high secondary yields for lower energy particles was given by Whipple.[18] An attempt to take advantage of materials with high secondary emission coefficients to influence spacecraft design to reduce charging was proposed by Rubin et al.[19]

16. Deutsch, M. -J., and Garrett, H. B. (1981) A "Worst Case" Charging Environment: Day 178, 1974, Unpublished manuscript.

17. Garrett, H. B., Schwank, D. C., Higbie, P. R., and Baker, D. N. (1980) Comparison Between the 30- to 80-keV Electron Channels on ATS6 and 1976-059A During Conjunction and Application to Spacecraft Charging Prediction, AFGL-TR-80-0124, AD 083476 and JGR, 85:115-1162.

18. Whipple, E. C. (1965) The Equilibrium Electric Potential of a Body in the Upper Atmosphere, NASA 615-65-296.

19. Rubin, A. G., Rothwell, P. L., and Yages, G. K. (1978) Reduction of spacecraft charging using highly emissive surface materials, in Effects of the Ionosphere on Space and Terrestrial Systems, edited by John M. Goodman, pp 313-316.

7. CONCLUSION

The parameters of interest for a "worst case" spacecraft charging environment are summarized in Table 7.

Table 7. A Geosynchronous Orbit "Worst Case" Environment Summary for Spacecraft Charging

Day:	24 April 1979		Satellite:	SCATHA	
Time:	~0651 UT (2311 MLT)		Regime:	Plasma Sheet	
R_E:	~6.6		L-shell:	~7.1	
Maximum Sunlight Charging Level: -340 V			Estimated Eclipse Charging Level: -16 kV		
Maximum Surface Material Charging Levels:			Quartz Fabric	-3.8 kV	
			Silvered Teflon	-6.4 kV	
			Aluminized Kapton	-1.5 kV	

2 Maxwellian Parameters (Least-Squares Fit):

Ions:		$n_1(cm^{-3})$	$n_2(cm^{-3})$	T_1(keV)	T_2(keV)
$\perp$	Mag Fld	1.1	1.3	0.3	28.2
$\parallel$	Mag Fld	1.6	0.6	0.3	26.0
Electrons:					
$\perp$	Mag Fld	0.2	2.3	0.4	24.8
$\parallel$	Mag Fld	0.2	0.6	0.4	24.0

Moments:

	n (cm^{-3})	NF (cm^{-2}-$s^{-1}$$sr^{-1}$)	ϵ (eV-cm^{-3})	EF (eV-cm^{-2}-s^{-1}-sr^{-1})	T_{AVE} (keV)	T_{RMS} (keV)
Ions:	2.3	2.0×10^8	1.9×10^4	5.4×10^{12}	0.55	14
Electrons:	0.9	4.7×10^9	9.6×10^3	8.4×10^{13}	7.7	9

Average $n(O^+)/n(H^+)$ [0.2-32 keV]: ~0.4 ± 0.1

The environment observed at ~0650 UT on 24 April 1979 has been shown to be a "worst case" environment but not necessarily "the worst case" environment since "worst case" is hard to define in terms of detrimental effects on different space systems. Spacecraft perform a wide range of functions and how those functions can be degraded depends heavily on the energy range, anisotropy, and composition of the particles to which they are most susceptible. Here we have examined an environment which produced one of the highest levels of sunlight and eclipse charging (φ_f)

observed during the first year of SCATHA operations. The ϕ_f in and of itself is not damaging to space systems, but the differential charging associated with it, can be. Various environmental parameters have been shown to be highly correlated with ϕ_f. Although the environment described above will seldom be encountered over a vehicle's lifetime, it is representative of the type of environment which can seriously degrade systems performance at geosynchronous orbit. It is recognized that SCATHA has yet to experience a super storm which might change current thinking on the limit of plasma sheet particle populations. However, until such time as that data might become available, 24 April 1979 ~0650 UT is a good example of a "worst case" environment.

References

1. Stevens, J. R., and Vampola, A. L. (Editors) (1978) Description of the Space Test Program P78-2 Spacecraft and Payloads, SAMSO-TR-78-24.
2. Hanser, F. A., Hardy, D. A., and Sellers, B. (1979) Calibration of the Rapid Scan Particle Detector Mounted in the SCATHA Satellite, AFGL-TR-79-0167, AD A082382.
3. DeForest, S. E. (1972) Spacecraft charging at synchronous orbit, JGR, 77:651-659.
4. UCSD Space Physics Lab Staff (1978) Handbook for UCSD SC9 SCATHA Auroral Particles Experiment, Unpublished.
5. Mizera, P. F., Leung, M. S., and Kan, H. K. A. (1980) Laboratory and Space Results From the SSPM Experiment, Aerospace Report No. TOR-0080(5505-02)-2.
6. Mizera, P. F., Koons, H. C., Schnauss, E. R., Croley, D. R., Jr., Kan, H. K. A., Lung, M. S., Stevens, N. J., Berkopec, F., Staskus, J., Lehn, W. L., and Nanewicz, J. E. (1981) First Results of Material Charging in the Space Environment, Aerospace Report No. TOR-0081(6506-01)-1.
7. Meng, C.-I. (1979) The Investigation of the Magnetospheric Dynamics in Conjunction With the SCATHA Satellite Observations, AFGL-TR-80-0070, AD A087433.
8. Ledley, B. G., Private communication.
9. Olson, W. P., and Pfitzer, K. A. (1974) A quantitative model of the magnetospheric magnetic field, JGR, 79:3739-3748.
10. Fennell, J. F., Private communication.
11. Kivelson, M. G., Kaye, S. M., and Southwood, D. J. (1979) The physics of plasma injection events, in Dynamics of the Magnetosphere, edited by S. I. Akasofu, 385-394, D. Reidel, Hingham, Massachusetts.
12. Johnson, R. G., Private communication.
13. Gordon Wrenn, Mullard, UCL, Private communication

14. Garrett, H. B. (1977) Modeling of the Geosynchronous Orbit Plasma Environment—Part 1, AFGL-TR-77-0288, AD A053164.

15. Sauvaud, J. -A., and Winckler, J. R. (1980) Dynamics of plasma energetic particles, and fields near synchronous orbit in the nighttime sector during magnetospheric substorms, JGR, 85:2043-2056.

16. Deutsch, M. -J., and Garrett, H. B. (1981) A "Worst Case" Charging Environment: Day 178, 1974, Unpublished manuscript.

17. Garrett, H. B., Schwank, D. C., Higbie, P. R., and Baker, D. N. (1980) Comparison Between the 30- to 80-keV Electron Channels on ATS6 and 1976-059A During Conjunction and Application to Spacecraft Charging Prediction, AFGL-TR-80-0124, AD 083476 and JGR, 85:115-1162.

18. Whipple, E. C. (1965) The Equilibrium Electric Potential of a Body in the Upper Atmosphere, NASA 615-65-296.

19. Rubin, A. G., Rothwell, P. L., and Yates, G. K. (1978) Reduction of spacecraft charging using highly emissive surface materials, in Effects of the Ionosphere on Space and Terrestrial Systems, edited by John M. Goodman, pp 313-316.